

Semi-infinite-geometry boundary problem for light migration in highly scattering media: a frequency-domain study in the diffusion approximation

Sergio Fantini,* Maria Angela Franceschini,* and Enrico Gratton

Laboratory for Fluorescence Dynamics, Department of Physics,
University of Illinois at Urbana-Champaign, 1110 West Green Street, Urbana, Illinois 61801-3080

Received December 13, 1993; revised manuscript received May 5, 1994

We have studied light migration in highly scattering media theoretically and experimentally, using the diffusion approximation in a semi-infinite-geometry boundary condition. Both the light source and the detector were located on the surface of a semi-infinite medium. Working with frequency-domain spectroscopy, we approached the problem in three areas: (1) we derived theoretical expressions for the measured quantities in frequency-domain spectroscopy by applying appropriate boundary conditions to the diffusion equation; (2) we experimentally verified the theoretical expressions by performing measurements on a macroscopically homogeneous medium in quasi-semi-infinite-geometry conditions; (3) we applied Monte Carlo methods to simulate the semi-infinite-geometry boundary problem. The experimental results and the confirming Monte Carlo simulation show that the diffusion approximation, under the appropriate boundary conditions, accurately estimates the optical parameters of the medium.

1. INTRODUCTION

Light propagation in turbid media is described by transport theory, also called the theory of radiative transfer.^{1,2} The Boltzmann transport equation, which is a balance relationship, treats light propagation as the transport of photons through a medium containing particles. In most practical cases the equation of transfer cannot be solved exactly. Often it is necessary to consider an approximate approach. One of these simplified approaches is the diffusion approximation,³⁻⁵ which is valid in the strongly scattering regime.⁶ The observed optical properties of most biological tissues⁷ are typified by a scattering coefficient that far exceeds the absorption coefficient. A number of studies employed the diffusion theory to investigate the optical properties of tissues. These studies used steady-state spectroscopy⁸⁻¹⁰ and time-resolved spectroscopy¹¹ in both the time domain¹²⁻¹⁴ and the frequency domain.¹⁵

We present a frequency-domain study of the applicability of the diffusion approximation to the case of a semi-infinite geometry. Both the light source and the detector are placed at the interface between air and a strongly scattering medium; the interface extends indefinitely. The proper solution of this boundary problem has important practical implications because it represents a reasonable model for *in vivo*, noninvasive applications of light spectroscopy in medicine. When the light source and the detector are placed on a surface separating two media with different optical properties, the diffusion approximation is not rigorously applicable.¹⁶ Nevertheless, the diffusion approximation has been applied to predict the time-domain and steady-state response in the reflectance geometry from quasi-semi-infinite tissues.^{10,12} We derive the expression for the frequency-domain photon fluence rate and verify its equivalence with the corresponding ex-

pression derived in the time domain.¹² Experimentally, we test the expression's level of accuracy by performing a systematic study on a macroscopically homogeneous tissue-like phantom. Since the diffusion theory is highly accurate in predicting the results of experiments performed in an infinite geometry,¹⁷⁻¹⁹ we compare our results obtained in the semi-infinite geometry (i.e., at the surface of the medium) with the results of the measurements conducted deep inside the bulk medium (i.e., in the infinite geometry). The comparison of experimental results is carried out for a wide range of values of μ_a and μ_s' . A Monte Carlo simulation of the boundary problem has been performed.

2. THEORY

The distribution of photons in random media is described by the angular photon density $u(\mathbf{r}, \Omega, t)$, which is defined so that $u(\mathbf{r}, \Omega, t)d^3r d\Omega$ is the expected number of photons in d^3r around \mathbf{r} moving in direction Ω in solid angle $d\Omega$ at time t . The temporal evolution of the angular photon density in a medium where the processes of absorption and elastic scattering take place is given by the Boltzmann transport equation⁴:

$$\frac{\partial u}{\partial t} = -\mathbf{v} \cdot \nabla u - v(\mu_a + \mu_s)u + \int_{4\pi} d\Omega' v\mu_s p_s(\Omega' \rightarrow \Omega) \times u(\mathbf{r}, \Omega', t) + q(\mathbf{r}, \Omega, t), \quad (1)$$

where \mathbf{v} is the speed of photons in the medium (and v its modulus), $v\mu_a$ and $v\mu_s$ are the rates of absorption and scattering, respectively, $p_s(\Omega' \rightarrow \Omega)$ is the normalized probability for scattering events that carry photons from Ω' into Ω , and q is the photon source term. The Boltzmann transport equation is an integrodifferential equation containing both time and spatial derivatives, and

its solution requires initial and boundary conditions for $u(\mathbf{r}, \Omega, t)$.

In the multiply scattering regime the usual simplification is the diffusion approximation. The approximation assumes that the angular photon flux, defined as $\psi(\mathbf{r}, \Omega, t) \equiv v u(\mathbf{r}, \Omega, t)$, is quasi-isotropic^{3,5}:

$$\psi(\mathbf{r}, \Omega, t) = \frac{1}{4\pi} \Psi + \frac{3}{4\pi} \mathbf{J} \cdot \Omega, \quad \left| \frac{\Psi}{3\mathbf{J} \cdot \Omega} \right| \gg 1, \quad (2)$$

where $\Psi(\mathbf{r}, t) \equiv \int_{4\pi} d\Omega \psi(\mathbf{r}, \Omega, t)$ is the total photon flux and $\mathbf{J}(\mathbf{r}, t) \equiv \int_{4\pi} d\Omega v u(\mathbf{r}, \Omega, t) \mathbf{\Omega}$ is the total photon current density. This assumption translates the transport equation [Eq. (1)] in a closed set of two equations for the total photon density $U(\mathbf{r}, t) \equiv \int_{4\pi} d\Omega u(\mathbf{r}, \Omega, t)$ and the total current density $\mathbf{J}(\mathbf{r}, t)$ (Ref. 4):

$$\frac{\partial U}{\partial t} + \nabla \cdot \mathbf{J} + v\mu_a U = q_0, \quad (3)$$

$$\frac{1}{v} \frac{\partial \mathbf{J}}{\partial t} + \frac{v}{3} \nabla U + (\mu_a + \mu_s') \mathbf{J} = \mathbf{q}_1, \quad (4)$$

where μ_s' [defined as $(1-g)\mu_s$, with g the average cosine of the scattering angle] is the transport scattering coefficient and q_0 and \mathbf{q}_1 are defined by introduction of the following expansion of the angular dependence of the source:

$$q(\mathbf{r}, \Omega, t) = \frac{1}{4\pi} q_0(\mathbf{r}, t) + \frac{3}{4\pi} \mathbf{q}_1(\mathbf{r}, t) \cdot \Omega. \quad (5)$$

If we assume that the photon source is isotropic ($\mathbf{q}_1 = 0$) and neglect the time derivative of \mathbf{J} , which is equivalent to saying that the variations of \mathbf{J} occur on a time scale much larger than the time between photon collisions with the scattering particles of the medium, Eq. (4) yields

$$\mathbf{J} = -vD\nabla U, \quad (6)$$

where $D = 1/(3\mu_a + 3\mu_s')$ is the diffusion constant. Finally, by using expression (6) for \mathbf{J} , we can rewrite Eq. (3) in the form of the photon-diffusion equation:

$$\frac{\partial U}{\partial t} - vD\nabla^2 U + v\mu_a U = q_0. \quad (7)$$

It is important to be clear about the limitations of the diffusion equation. As is discussed, its derivation requires the following approximations:

- (a) Quasi-isotropic angular photon flux [Eq. (2)];
- (b) Isotropic photon source [$\mathbf{q}_1 = 0$ in Eqs. (4) and (5)];
- (c) Time variations of \mathbf{J} that are slow with respect to the photon mean collision time [$\partial \mathbf{J} / \partial t$ neglected in Eq. (4)].

It has been shown that the photon-flux quasi-isotropy condition is well satisfied^{6,16}

- (a1) In strongly scattering media ($\mu_a \ll \mu_s'$),
- (a2) Far from boundaries,
- (a3) Far from sources,

where "far" in conditions (a2) and (a3) refers to distances much greater than the photon mean free path.

In frequency-domain spectroscopy the intensity of the

light source is modulated at a frequency ($\omega/2\pi$) typically of tens to hundreds of megahertz, so the photon density is written as

$$U = U_{dc} + U_{ac} \exp[-i(\omega t - \phi)],$$

where U_{dc} , U_{ac} , and $(\phi - \omega t)$ are the dc component, the amplitude of the ac component, and the phase, respectively. When we consider a homogeneous infinite medium and assume a source term in the form of $q_0 = S\delta(\mathbf{r})[1 + A \exp(-i\omega t)]$, where $\delta(\mathbf{r})$ is the Dirac function, S is the source strength in photons per second, and A is the modulation of the source, the following results for the frequency domain quantities are derived from Eq. (7) (Ref. 20):

$$U_{dc} = \frac{S}{4\pi v D} \frac{\exp\left[-r\left(\frac{\mu_a}{D}\right)^{1/2}\right]}{r}, \quad (8)$$

$$U_{ac} = \frac{SA}{4\pi v D} \frac{\exp\left[-r\left(\frac{\mu_a}{2D}\right)^{1/2} [(1+x^2)^{1/2} + 1]^{1/2}\right]}{r}, \quad (9)$$

$$\phi = r\left(\frac{\mu_a}{2D}\right)^{1/2} [(1+x^2)^{1/2} - 1]^{1/2}, \quad (10)$$

where ϕ is the phase lag between the source (located at $\mathbf{r} = 0$) and the detector (located at a distance $r \gg 1/\mu_s'$ from the source) and x is defined as $\omega/v\mu_a$, with v the speed of light in the medium (given by c/n , with n being the index of refraction of the medium). Equations (8)–(10) have been experimentally verified^{11,19–21} and provide a good description of the homogeneous infinite medium problem in the multiply scattering regime.

In most medical applications the method for noninvasive, *in vivo* spectroscopy measurements is to place both the light source and the detector upon the surface to be examined. It is evident that the infinite-medium scheme is not appropriate for such a geometry. A better approach is to consider a uniform semi-infinite medium and to solve the diffusion equation [Eq. (7)] with the appropriate boundary conditions. Before proceeding, we note that the problem itself is beyond the limits of the diffusion approximation: both source and detector are placed on the boundary, where, as discussed, the diffusion equation does not approximate the transport equation as well as it does deep in the medium. However, it is still a reasonable starting point to treat the problem,¹² even if the final results must be critically analyzed to verify the extent of acceptability. The validity of the diffusion approximation can be quantified by evaluation of the ratio between the isotropic and the directional photon flux. This ratio should be much greater than 1, as is required by relation (2). In the homogeneous infinite medium, where the diffusion approximation yields accurate results, for typical values of the physical parameters of tissue in the near infrared ($\mu_a = 0.05 \text{ cm}^{-1}$, $\mu_s' = 15 \text{ cm}^{-1}$, $r = 3 \text{ cm}$, $v = 2.26 \times 10^{10} \text{ cm/s}$, corresponding to an index of refraction of $n = 1.33$, and $\omega = 2\pi \times 120 \text{ MHz}$) such a ratio is

$$\left| \frac{\Psi}{3\mathbf{J} \cdot \Omega} \right| \equiv \left| \frac{vU}{3vD\nabla U \cdot \Omega} \right| > \frac{U}{3D|\nabla U|} \approx 8. \quad (11)$$

The physical boundary condition required at a vacuum interface is that there be no incoming photons at the boundary.⁴ Apparently at the vacuum boundary the diffusion approximation breaks down. The photon flux is nonzero only on half of the range of the solid angle, and the quasi-isotropy condition is not satisfied. On the other hand, a mismatch of the index of refraction at the interface of the strongly scattering medium and the outside nonscattering medium accounts for an inwardly directed component of the photon flux at the boundary. The boundary condition for the mismatch semi-infinite medium can be satisfied when the density of photons U is equal to 0 on an extrapolated boundary at a distance $z_b = 2aD$, where a is a constant that is related to the relative index of refraction (n_{rel}) of the two media.^{22,23} The distance z_b for $n_{rel} = 1.33$ (or $n_{rel} = 1.4$, which is a typical value for a tissue-air interface in the red-near-infrared spectral region²⁴) and for typical values of D in tissues is ~ 0.15 cm. Furthermore, it has been shown that a light beam incident upon the surface can be well represented by a single scatter source at a depth z_0 equal to one effective photon mean free path^{10,12} [i.e., $z_0 = 1/(\mu_a + \mu_s')$]. This parameter z_0 has a value of ~ 0.1 cm in tissues. We observe that this feature accounts for an effective isotropic photon source even if the photons are actually injected in a single direction. Finally, the boundary problem of setting $U = 0$ on the extrapolated boundary can be treated by introduction of a negative image source of photons above the plane, one that is symmetric with respect to the actual photon source.²⁵ This approach enables one to take advantage of the solution that is valid for the infinite medium. In the semi-infinite-medium model, which is pictorially represented in Fig. 1, the diffusion equation [Eq. (7)] is used with $q_0 = q_a - q_i$ (where a stands for the actual source and i stands for the image) to yield the solution obeying the required boundary conditions in the space $z \geq z_b$. The solution, by application of the superposition principle, can immediately be written from expressions (8)–(10):

where, with the notation introduced in Fig. 1,

$$r_a = \rho \left[1 + \left(\frac{z_b + z_0 - z}{\rho} \right)^2 \right]^{1/2},$$

$$r_i = \rho \left[1 + \left(\frac{z_b + z_0 + z}{\rho} \right)^2 \right]^{1/2}.$$

The new coordinate ρ is the projection of the source-detector distance r_a on the interface plane $z = z_b$. The detector coordinate z is at $z_b \leq z \leq z_b + z_0$. Assuming that $1 \gg (z_b + z_0 \pm z)^2/\rho^2$, in Eq. (12) we carry over expansions to the second order in $(z_b + z_0 \pm z)/\rho$. After the necessary calculations, using Eqs. (12), (2), and (6), we find that the dc and ac photon flux along $-z$ (in Fig. 1 the detector fiber receives photons in an inward direction $-z$) and the phase lag ϕ^s between source and detector are given by the following relationships:

$$\psi_{dc}^s = \frac{2S}{(4\pi)^2 D} \frac{\exp \left[-\rho \left(\frac{\mu_a}{D} \right)^{1/2} \right]}{\rho^3} \times \left[1 + \rho \left(\frac{\mu_a}{D} \right)^{1/2} \right] (z_b + z_0) \times \left(z + 3D \left\{ 1 - \frac{(z_b + z_0)^2 + 3z^2}{2\rho^2} \right\} \right) \times \left\{ \left[3 + \frac{\rho^2 \frac{\mu_a}{D}}{1 + \rho \left(\frac{\mu_a}{D} \right)^{1/2}} \right] \right\}, \quad (13)$$

$$U^s = \frac{S}{4\pi v D} \left[\frac{\exp \left[-r_a \left(\frac{\mu_a}{D} \right)^{1/2} \right]}{r_a} - \frac{\exp \left[-r_i \left(\frac{\mu_a}{D} \right)^{1/2} \right]}{r_i} \right] + \frac{SA}{4\pi v D} \frac{\exp \left[-r_a \left(\frac{\mu_a}{2D} \right)^{1/2} \right] \{ [(1 + x^2)^{1/2} + 1]^{1/2} - i[(1 + x^2)^{1/2} - 1]^{1/2} \}}{r_a} - \frac{\exp \left[-r_i \left(\frac{\mu_a}{2D} \right)^{1/2} \right] \{ [(1 + x^2)^{1/2} + 1]^{1/2} - i[(1 + x^2)^{1/2} - 1]^{1/2} \}}{r_i} \exp(-i\omega t), \quad (12)$$

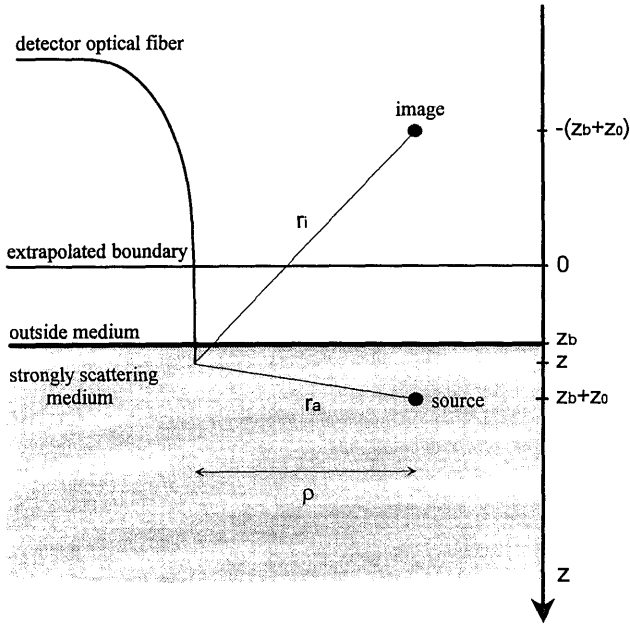


Fig. 1. Semi-infinite-geometry model: z_b is the distance between the extrapolated boundary and the surface of the medium and z_0 is the depth of the effective single scatter source inside the scattering medium. The strongly scattering medium extends in the space $z > z_b$. The detector optical fiber, which is parallel to the z axis, is immersed in the scattering medium at a depth z ranging from z_b to $z_b + z_0$. The distance between the effective (image) photon source and the tip of the optical fiber is r_a (r_i). The projection of the source-detector distance onto the plane $z = 0$ is ρ .

where

$$V^+ = [(1 + x^2) + 1]^{1/2}, \quad V^- = [(1 + x^2) - 1]^{1/2},$$

and, as previously defined,

$$x = \frac{\omega}{v\mu_a}.$$

The superscript s stands for surface measurement. The specific conditions imposed to yield Eqs. (13)–(15) are

$$\frac{1}{8} \rho^2 \frac{\mu_a}{D} \left(\frac{z_b + z_0 + z}{\rho} \right)^4 \ll 1, \quad (16)$$

$$\frac{1}{8} \rho^2 (V^+)^2 \frac{\mu_a}{2D} \left(\frac{z_b + z_0 + z}{\rho} \right)^4 \ll 1, \quad (17)$$

$$\frac{1}{2} \rho^2 \left(\frac{\mu_a}{D} \right)^{1/2} V^- \frac{(z_b + z_0)^2 + 3z^2}{\rho^2} \ll 1. \quad (18)$$

In tissues, conditions (16) and (17) are better satisfied than condition (18). For the previously mentioned tissue's optical properties in the near-infrared, the quantities on the left-hand sides of inequalities (16) and (17) are ~ 0.001 , and that on the left-hand side of inequality (18) is ~ 0.01 .

We have compared our result for the frequency-domain quantities with the expression for the time-domain reflectance in the half-space geometry obtained by Patterson *et al.*¹² Since the same boundary conditions have been applied, the two solutions should be related by a Fourier transform with respect to time. We have verified the correspondence of the two results in the limiting case $(z_b/\rho) = (z_0/\rho) = (z/\rho) = 0$. We denote the time-domain and the frequency-domain photon current densities by $\mathbf{J}(\rho, t)$ and $\tilde{\mathbf{J}}(\rho, \omega)$, respectively; the expressions derived by Patterson *et al.* for $\mathbf{J}(\rho, t)$ and the one derived in this paper for $\tilde{\mathbf{J}}(\rho, \omega)$ {given by $\tilde{\mathbf{J}}_{ac}(\rho, \omega) \exp[i\Phi(\rho, \omega)]$ } obey the following relationship:

$$\int_{-\infty}^{+\infty} |\mathbf{J}(\rho, t)| \exp(i\omega t) dt = |\tilde{\mathbf{J}}(\rho, \omega)|. \quad (19)$$

This relationship, showing a Fourier correlation, states the equivalence of the solutions derived in the time and the frequency domains.

To verify experimentally the solutions found for the semi-infinite geometry and to use the measurement protocol described in a previous paper,¹⁹ we rewrite Eqs. (13)–(15) to obtain quantities that show a linear dependence on ρ :

$$\ln \left[\frac{\rho^3 \psi_{dc}^s}{\left[1 + \rho \left(\frac{\mu_a}{D} \right)^{1/2} \right] F_{dc}(\rho, \mu_a, D, z_b, z_0, z)} \right] = -\rho \left(\frac{\mu_a}{D} \right)^{1/2} + G_{dc}(D, S, z_b, z_0), \quad (20)$$

$$\psi_{ac}^s = \frac{2SA}{(4\pi)^2 D} \frac{\exp \left[-\rho \left(\frac{\mu_a}{2D} \right)^{1/2} V^+ \right]}{\rho^3} \times \left\{ 1 + \rho \left(\frac{2\mu_a}{D} \right)^{1/2} V^+ + \rho^2 \frac{\mu_a}{D} (1 + x^2)^{1/2} \right\}^{1/2} \times (z_b + z_0) \left(z + 3D \right) \left[1 - \frac{(z_b + z_0)^2 + 3z^2}{2\rho^2} \right] \times \left[2 + \frac{1 + \rho \left(\frac{\mu_a}{2D} \right)^{1/2} V^+}{1 + \rho \left(\frac{2\mu_a}{D} \right)^{1/2} V^+ + \rho^2 \frac{\mu_a}{D} (1 + x^2)^{1/2}} \right] + \left[\rho \left(\frac{\mu_a}{2D} \right)^{1/2} V^+ \right] \left(\right), \quad (14)$$

$$\Phi^s = \rho \left(\frac{\mu_a}{2D} \right)^{1/2} V^- - \arctan \left[\frac{\rho \left(\frac{\mu_a}{2D} \right)^{1/2} V^-}{1 + \rho \left(\frac{\mu_a}{2D} \right)^{1/2} V^+} \right], \quad (15)$$

$$\ln \left[\frac{\rho^3 \psi_{dc}^s}{\left[1 + \rho \left(\frac{2\mu_a}{D} \right)^{1/2} V^+ + \rho^2 \frac{\mu_a}{D} (1 + x^2)^{1/2} \right]^{1/2} F_{ac}(\rho, \mu_a, D, \omega, v, z_b, z_0, z)} \right] = -\rho \left(\frac{\mu_a}{2D} \right)^{1/2} V^+ + G_{ac}(D, S, A, z_b, z_0), \quad (21)$$

$$\Phi^s + \arctan[F_{\Phi}(\rho, \mu_a, D, \omega, v)] = \rho \left(\frac{\mu_a}{2D} \right)^{1/2} V^-, \quad (22)$$

where the ρ -dependent functions F_{dc} , F_{ac} , and F_{Φ} and the ρ -independent functions G_{dc} and G_{ac} are defined by Eqs. (13)–(15). The determination of the slopes of the straight lines allows one to recover the values of μ_a and μ_s' of the medium. That the arguments of the logarithms are not dimensionless does not present a problem as far as the slopes of the straight lines are concerned. In fact the particular choice of the units introduces a constant, which does not effect the slopes. We also observe that the particular values of the parameters of the model (namely, z_b , z_0 , and z) have no influence on the slopes of the lines (z has no effect on their intercept either). This property is important, because the parameters z_b and z_0 depend on the optical properties of the medium, namely, on μ_s' and n , and the positioning of the tip of the detector optical fiber (which is related to the parameter z) is in practice not exactly reproducible.

We conclude this theoretical section by observing that the isotropy factor defined by Eq. (11), for the same values of the parameters considered in Eq. (11), has a minimum value of ~ 2 , which is marginally acceptable compared with the value of 8 in the infinite geometry. This result indicates that the isotropic term is larger than the directional flux but is not much larger as required by the diffusion approximation. We evaluate the level of accuracy of the semi-infinite-medium expression (13) by performing a series of measurements in a macroscopically homogeneous, strongly scattering medium and by a Monte Carlo simulation.

3. EXPERIMENTAL METHODS

The experimental arrangement, shown in Fig. 2, is typical for frequency-domain spectroscopy. The light source, a diode laser (Sony SLD104AU) emitting at a wavelength of 780 nm, is intensity modulated at a frequency of 120 MHz by being supplied with the sine-wave output of a frequency synthesizer (Marconi 2022A) by means of an rf amplifier (ENI Model 403 LA). The average emitted light power is ~ 3 mW. In our measurements the laser diode is directly immersed in the medium, and the detected light is collected by a bundle of optical fibers (overall diameter 3 mm) and delivered to a photomultiplier tube (PMT) (Hamamatsu R928). The gain function of the PMT is modulated at a frequency of 120.00008 MHz, which is slightly different from the modulation frequency of the light source. The small frequency difference, which is selectable, produces beating between the detected signal and the gain function of the PMT, giving rise to a signal at the difference

frequency (80 Hz in our case), which is sent to a computer card. A digital acquisition technique²⁶ and a fast-Fourier-transform algorithm provide the phase shift relative to a reference signal (Φ), the average intensity (dc), and the amplitude of the intensity oscillations (ac) of the detected light. The signal used as a reference for the phase measurement is a synchronous (with the frequency synthesizer) clock generated by the computer.

The multiply scattering medium used in our measurement is an aqueous solution of Liposyn III 10% [Abbott Laboratories (IL)]. It is an intravenous fat emulsion that was previously used as tissue-like phantom in both steady-state¹⁰ and time-resolved spectroscopy.²⁷ We studied four different Liposyn concentrations to test the theoretically derived results in a range of values for μ_s' . The concentrations employed are 4.5%, 9.0%, 13.5%, and 18% by volume, which correspond to a solids content of 0.45%, 0.90%, 1.35%, and 1.80%, respectively. Consequently the transport scattering coefficient μ_s' should range from ~ 4 to 16 cm⁻¹, as we verified with measurements in the infinite medium before performing the surface experiment. The aqueous Liposyn solution acts as the host medium, diluting the absorbing substance. For such a substance we chose black India ink, which is soluble in water. We measured its absorption spectrum in a non-scattering regime at the wavelength of the diode laser (780 nm) with a standard spectrophotometer (Perkin-Elmer Lambda 5). The result, relative to a dilution of 0.2 mL of a prediluted India-ink solution in 1 L of water, is $\mu_a = (0.0143 \pm 0.0005)$ cm⁻¹. On the basis of this re-

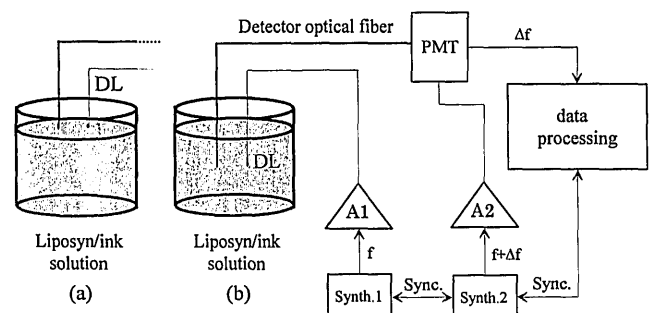


Fig. 2. Experimental arrangement showing the two source-detector configurations used in (a) the semi-infinite geometry and (b) the infinite geometry. In (a) the source and the detector are at the surface, and in (b) they are immersed in the medium. Diode laser DL is modulated by synthesizer Synth.1 (frequency $f = 120$ MHz) through rf amplifier A1. The detector light is collected by a bundle of optical fibers coupled to a PMT, whose gain function is modulated at frequency $f + \Delta f = 120$ MHz + 80 Hz by synthesizer synth.2 via amplifier A2. The output signal of the PMT (frequency $\Delta f = 80$ Hz) is sent to a computer card for processing. Synth.1, synth.2, and the computer card are all synchronized. Sync.'s, reference signals (synchronous clock).

sult we decided to increase the concentration of absorber at steps of 0.2 mL/L to increase μ_a by 0.014 cm^{-1} per step. After the first 10 steps we increased the amount of absorber added between successive measurements. We performed 24 measurements in 24 different conditions of scatterer and absorber contents. First we increased the transport scattering coefficient (measurements 1–4, μ_s' ranging from ~ 4 to 16 cm^{-1}); then we increased the absorption coefficient without changing the scatterer solids content (measurements 5–24, μ_a ranging from ~ 0.026 to 0.4 cm^{-1}). The solution was held in a cylindrical container (22 cm in diameter by 13 cm in height).

Our measurement protocol consists of two series of measurements for each Liposyn–black-India-ink solution. The first series is conducted in the quasi-infinite geometry (shortened to infinite geometry in what follows), in which both the light source and the detector optical fiber are deeply immersed into the medium (at a depth of ~ 5 cm). The second series is performed in the quasi-semi-infinite geometry (shortened to semi-infinite geometry), in which both the light source and the detector optical fiber are positioned on the surface of the medium. In each one of the two series of measurements we collect data at 5–8 different source–detector separations, ranging from a minimum of 1.6 cm to a maximum of 5.4 cm. The different source–detector separations are accomplished by means of a raster scanning device (Techno XYZ positioning table), which moves the light source with respect to the fixed-detector optical fiber. The uncertainty in the variations of r (or ρ) is $\sim 10 \mu\text{m}$. The experimental configurations in the infinite and semi-infinite geometries are sketched in Fig. 2. We observe that the source–detector separations are measured from the emitting point of the laser diode to the center of the detector fiber bundle. The effect of the finite size of the detector fiber (3 mm in diameter) on the measured values of μ_a and μ_s' is negligible when multiple source–detector distances are employed in the data analysis. We have experimentally verified that fibers with different diameters give the same values of μ_a and μ_s' .

The measurement of dc, ac, and phase at several source–detector distances enables us to determine the slopes of the straight lines associated with dc (S_{dc}), ac (S_{ac}), and phase (S_ϕ). These straight lines are given by $\ln(rU_{dc})$, $\ln(rU_{ac})$, and Φ in the infinite geometry²⁰ and by Eqs. (20)–(22) in the semi-infinite geometry. In the infinite geometry the way to recover μ_a and μ_s' has been described in detail.¹⁹ In the semi-infinite geometry we treat the problem of recovering μ_a and μ_s' from Eqs. (20)–(22) iteratively: First we neglect the terms containing μ_a and μ_s' on the left-hand side of the equations and obtain the slopes $S_{dc}^{(0)}$, $S_{ac}^{(0)}$, and $S_\phi^{(0)}$ from which we determine $\mu_a^{(0)}$ and $\mu_s^{(0)}$. Then we use these values to obtain $S_{dc}^{(1)}$, $S_{ac}^{(1)}$, and $S_\phi^{(1)}$ and hence $\mu_a^{(1)}$ and $\mu_s^{(1)}$, and we continue applying this procedure recursively until $\mu_a^{(i)}$ and $\mu_s^{(i)}$ reproduce themselves within a given uncertainty of 0.1%. The convergence is reached after few iterations.

4. EXPERIMENTAL RESULTS

On the basis of the discussion conducted in an earlier paper¹⁹ we have recovered μ_a and μ_s' from the data pairs of dc and phase and ac and phase. In what follows we

present only the results obtained from dc and phase data, but we note that similar results are obtained from ac and phase data.

Infinite Geometry

The values of μ_s' and μ_a measured in the infinite geometry are plotted in Fig. 3 as a function of Liposyn and black-ink concentrations. In Fig. 3(a1), μ_s' shows a linear dependence on the scatterer-solids content, in agreement with linear transport theory.³ By contrast, μ_s' is essentially insensitive to the increase in the black-ink concentration [Fig. 3(a2)]. In the absence of black ink, the measured value of μ_a for diluted Liposyn ($0.026 \pm 0.001 \text{ cm}^{-1}$) is essentially due to water. In fact, the reported value²⁸ of μ_a for water at 780 nm, which is 0.023 cm^{-1} , is in good agreement with our measurement. The linear dependence of μ_a on black-ink concentration [Fig. 3(b2)] is also in agreement both with the theory ($\mu_a = \epsilon[c]$, where ϵ is the extinction coefficient and $[c]$ is the chromophore concentration) and with other

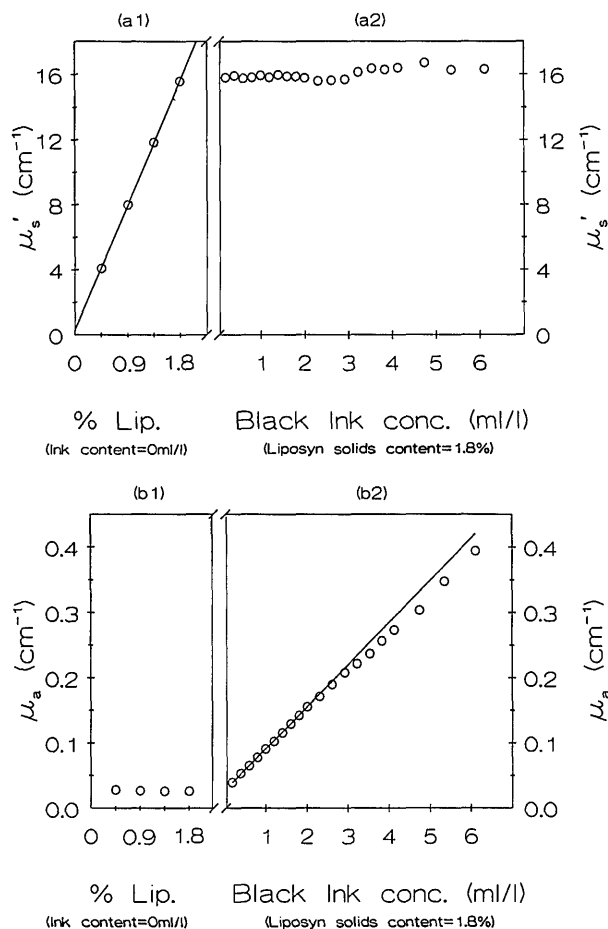


Fig. 3 Results of the infinite-geometry measurements relative to the various concentrations of Liposyn and black India ink. In (a1) and (b1) the x axis indicates the Liposyn solids content (%) at constant black-India-ink concentration (0 mL/L), and in (a2) and (b2) the x axis shows black-India-ink concentrations (mL/L) at constant Liposyn solids content (1.8%). In all the panels the error bars are of the order of the symbol dimensions or smaller. (a1), (a2) μ_s' , the straight line through the points relative to different Liposyn solids content is obtained by a linear least-squares fit. (b1), (b2) μ_a , the straight line, obtained by a linear least-squares fit, has been calculated with the points relative to ink concentrations smaller than 2 mL/L (see Section 6).

experiments.^{17,19} The slope of the straight line calculated with the points relative to ink concentrations smaller than 2 mL/L [$(64.5 \pm 0.4) \times 10^{-3} \text{ cm}^{-1} \text{ mL}^{-1} \text{ L}$], for which the diffusion theory provides an excellent approximation to the transport theory, is very close to the slope obtained spectrophotometrically in a nonscattering regime [$(66.1 \pm 0.3) \times 10^{-3} \text{ cm}^{-1} \text{ mL}^{-1} \text{ L}$]. The measured values of μ_a relative to ink concentrations greater than 2 mL/L deviate from the values measured on the spectrophotometer by less than 6%. On the basis of these observations we assume that the infinite-geometry measurements provide accurate results for the optical parameters of the medium. We therefore use these results as reference values for the semi-infinite-geometry measurements

Semi-infinite Geometry

We have analyzed the surface data in two ways: (i) considering Eqs. (20)–(22), thereby taking into account the appropriate boundary conditions, and (ii) using the infinite-geometry equations (8)–(10). In these ways we quantify the corrections yielded by the application of the proper boundary conditions with respect to the infinite-geometry results. The results for μ_s' and μ_a in the 24 media variations examined are shown in Fig. 4, where they may be compared with the results of the infinite-geometry measurements. We have also compared the values of the slopes related to dc (S_{dc}), ac (S_{ac}), and phase (S_ϕ) in the three cases considered (referred to as the infinite geometry, the semi-infinite geometry with boundary conditions, and the semi-infinite geometry without boundary conditions). This comparison, plotted in Fig. 5, provides information on the behavior of the frequency-domain parameters, namely, on their deviation from the accurate infinite-model predictions.

The sensitivity of the semi-infinite-geometry results to the positioning of the source and the detector relative to the surface plane can be evaluated by comparison of the data presented in Table 1. We measured the values of μ_a and μ_s' for slightly different positions of the laser diode and the tip of the detector optical fiber. That is, assigning to the medium surface a coordinate $\zeta = 0$, we have examined two positions relative to the boundary plane, i.e., a surface position ($\zeta = 0$) and 1 mm into the medium ($\zeta = 1$). We then obtained four possible configurations for the source–detector system, that is, (0, 0), (1, 0), (0, 1), and (1, 1), where the first coordinate is relative to the source and the second is relative to the detector. Table 1 shows the results obtained for μ_a and μ_s' in the solution with 1.8% of Liposyn and 0.4 mL/L of ink in the four configurations described by analysis of the data with Eqs. (20)–(22), i.e., taking into account for proper boundary conditions.

5. MONTE CARLO SIMULATION

To obtain a result free of possible experimental artifacts, we have implemented a Monte Carlo simulation program. A point source of photons is simulated, and the trajectory history of each photon is traced through a homogeneous cubic lattice in which each cell is associated with the same probability of absorption and scattering. A random-number generator samples the possible

physical events on the basis of probability distributions related to the values of the optical parameters in the medium. A fast Fourier transform of the time distribution of photons at each lattice site provides the frequency-domain equivalent of an intensity-modulated point source at multiple frequencies. The semi-infinite-geometry boundary conditions are applied in the following way: when a photon reaches a coordinate $\zeta < 0$, where $\zeta = 0$ is the interface plane on which the source and detector are placed, it is absorbed. In this way we simulate the loss of photons through the air–liquid interface. We have run this frequency-domain Monte Carlo simulation for source–detector separations ranging from 3 to 10 cm and used the following values of the optical parameters of the medium: $\mu_a = 0.059 \text{ cm}^{-1}$, $\mu_s' = 3.2 \text{ cm}^{-1}$, and $n = 1.33$. For these values of the parameters the size of the Monte Carlo lattice is large enough to prevent photon escape. The number of photon histories traced is 2×10^8 . The simulation ran on a 486-66 MHz IBM-compatible PC in ~ 10 h. The number of detected photons is large enough to provide good statistics. In the infinite (semi-infinite) geometry we detected approximately 9×10^6 (5×10^6) and 13×10^3 (2.4×10^3) for source–detector separations of 3 and 10 cm, respectively.

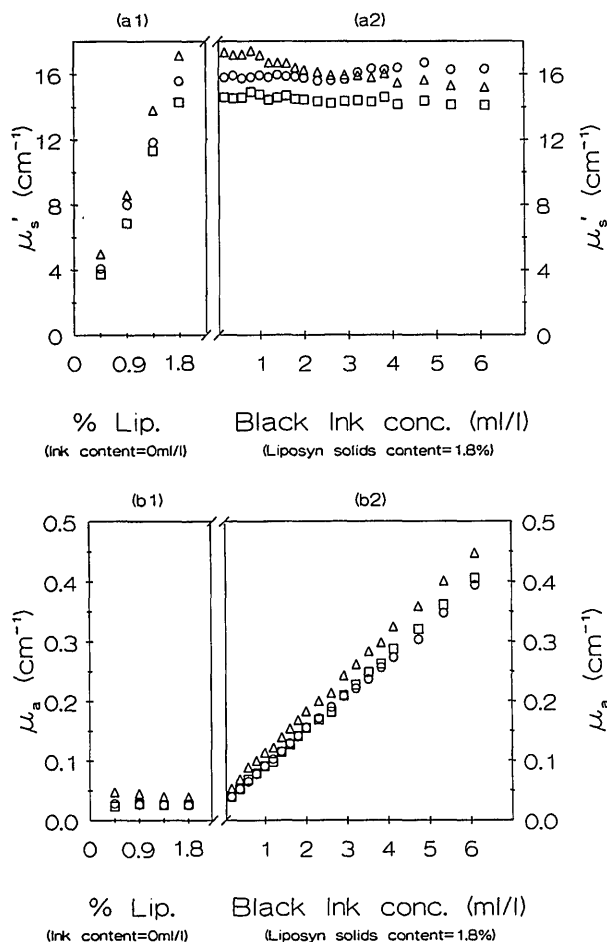


Fig. 4. Comparison of the values of (a1), (a2) μ_s' and (b1), (b2) μ_a measured in the three cases considered: circles, infinite geometry; squares, semi-infinite geometry with boundary conditions; triangles, semi-infinite geometry without boundary conditions. The conditions for the x axis are described in the caption of Fig. 3. The error bars are of the order of the symbol dimensions or smaller.

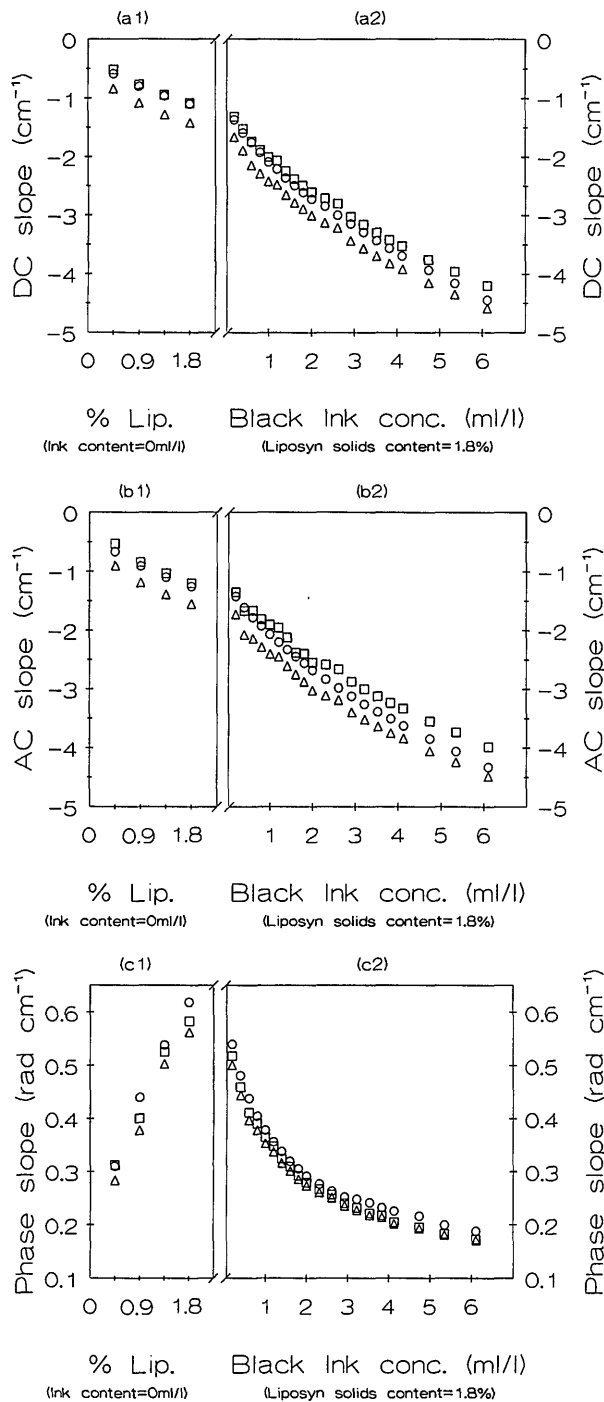


Fig. 5. Comparison of the slopes associated with (a1), (a2) dc intensity; (b1), (b2) ac intensity; and (c1), (c2) phase, measured for different Liposyn and ink concentrations in the three cases considered: circles, infinite geometry; squares, semi-infinite geometry with boundary conditions; triangles, semi-infinite geometry without boundary conditions. The conditions for the x axis are described in the caption of Fig. 3.

The results of the Monte Carlo simulation for a modulation frequency of 120 MHz (to match the experimental modulation-frequency condition) are shown in Fig. 6 and Table 2. In Fig. 6 we show a comparison of the straight lines associated with dc, ac, and phase in the case of the infinite geometry, the semi-infinite geometry with boundary conditions, and the semi-infinite geometry without

boundary conditions. In Table 2 we list the values obtained for μ_a and μ_s' in the three cases.

6. DISCUSSION

Infinite-Geometry Results

The infinite-geometry results shown in Fig. 3 have been used as a framework to provide the correct values of the optical parameters in the multiply scattering medium. Several arguments have been presented above justify this designation:

- (i) The linear dependence of μ_s' on Liposyn solids content;
- (ii) The independence of μ_s' from black-India-ink concentration;
- (iii) The independence of μ_a from Liposyn solids content;
- (iv) The linear dependence, quantitatively similar to the one obtained spectrophotometrically, of μ_a on black-India-ink concentration.

Whereas conditions (i) and (iii) are certainly well satisfied, conditions (ii) and (iv) hold rigorously only for black-India-ink concentrations smaller than ~ 3 mL/L. However, the deviations of the measured values of μ_s' and μ_a at the maximum ink concentration examined (6.1 mL/L) from the values that would satisfy conditions (ii) and (iv) are small ($\sim 6\%$). We neglected these deviations in comparing the semi-infinite-geometry results. From a general standpoint these deviations are a sign of the shortcomings of the diffusion approximation for higher absorption coefficients. As discussed in Section 2, the diffusion approximation requires μ_s'/μ_a to be much greater than 1. The results of our measurements permit us to quantify this requirement: the values of the optical parameters of our medium are consistent with Mie theory and with spectrophotometric measurements when $\mu_s'/\mu_a > 80$, and they deviate by $\sim 6\%$ for $\mu_s'/\mu_a \approx 40$.

Semi-infinite-Geometry Results

The method used to recover the values of μ_a and μ_s' from the measured data is based on the determination of the slopes of the straight lines associated with dc, ac, and phase. In the semi-infinite geometry this method presents the advantage of being insensitive to the values of the distance parameters of the model, z_b , z_0 , and z . This topic was discussed in Section 2 on the basis of the derived expressions for the dc, the ac, and the phase slopes. The results presented in Table 1 experimentally confirm the theoretical predictions relative to the parameter z . Therefore the combined theoretical and experimental results show that the relative index of refraction (influencing z_b), the value of the photon mean free path in the multiply scattering medium (related to z_0), and

Table 1. Sensitivity to Source-Detector Positioning on the Surface

Depth of Immersion (mm)		μ_a (cm $^{-1}$)	μ_s' (cm $^{-1}$)
Source	Detector		
0	0	0.053 ± 0.001	14.5 ± 0.4
1	0	0.052 ± 0.001	14.9 ± 0.4
0	1	0.053 ± 0.001	14.7 ± 0.4
1	1	0.051 ± 0.001	14.8 ± 0.4

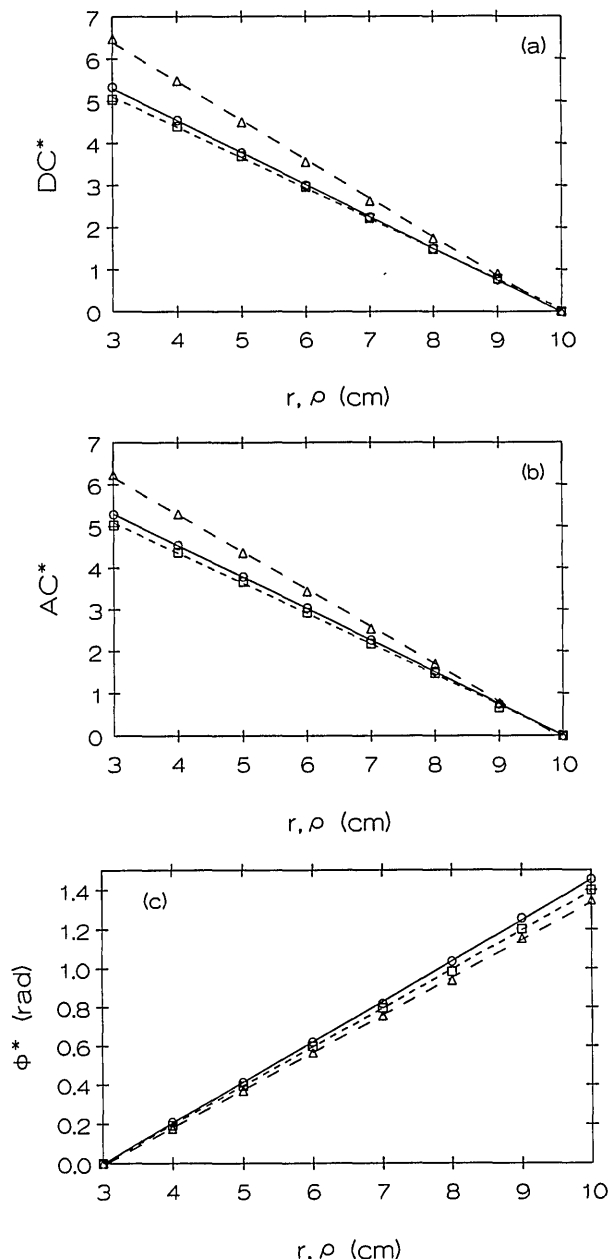


Fig. 6. Straight lines associated with (a) dc, (b) ac, and (c) phase as a function of r (infinite geometry) or ρ (semi-infinite geometry), obtained from the Monte Carlo simulation. The different symbols refer to the three conditions examined (dc* and ac* refer to values relative to the maximum source-detector distance and Φ^* refers to a value relative to the minimum source-detector distance). Circles, infinite-medium simulation, infinite-geometry equations: $dc^* = \ln(rU_{dc})$, $ac^* = \ln(rU_{ac})$, $\Phi^* = \Phi$. Squares, semi-infinite-medium simulation, semi-infinite-geometry equations: dc^* , ac^* , and Φ^* given by the left-hand sides of Eqs. (20)–(22). Triangles, semi-infinite-medium simulation, infinite-geometry equations: $dc^* = \ln(\rho\psi_{dc}^s)$, $ac^* = \ln(\rho\psi_{ac}^s)$, $\Phi^* = \Phi^s$.

the position of the fiber relative to the boundary surface (given by z) are not critical parameters. Their values can change without substantially affecting the results of a measurement. However, it should be stressed that this statement is true only within the model constraints, i.e., when the conditions $z_b \leq z \leq z_b + z_0$ and $1 \gg (z_b + z_0 \pm z)^2/\rho^2$ are satisfied. The experimental straight-

line parameters considered in this paper are obtained by least-squares fits. In all cases considered the linear fits are very good; the correlation coefficients typically exceed 0.999.

The comparison of the measured values of μ_a and μ_s' in the three cases considered (infinite geometry, semi-infinite geometry with boundary conditions, and semi-infinite geometry without boundary conditions) is presented in Fig. 4. A more quantitative comparison is made by analysis of the deviations of the semi-infinite geometry results from the infinite-geometry results. These deviations are shown in Fig. 7. With proper boundary conditions the semi-infinite measurements yield values of μ_a that differ by less than 4% from the values determined with the infinite geometry. The deviations relative to μ_s' are larger, ranging from ~5% to 15%, but

Table 2. Monte Carlo Simulation Results

Geometry	μ_a (cm ⁻¹)	μ_s' (cm ⁻¹)
Infinite	0.0586 ± 0.0004	3.22 ± 0.03
Semi-infinite with boundary conditions	0.0580 ± 0.0007	2.95 ± 0.06
Semi-infinite without boundary conditions	0.077 ± 0.001	3.6 ± 0.1

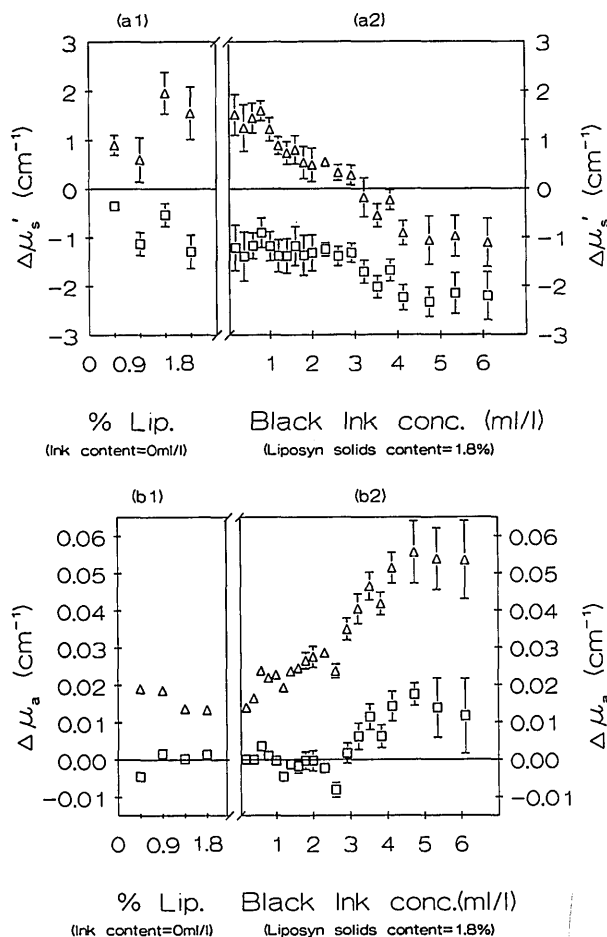


Fig. 7. Differences between the values of (a1), (a2) μ_s' and (b1), (b2) μ_a measured in the semi-infinite geometry and those obtained in the infinite geometry: squares, with boundary conditions; triangles, without boundary conditions. The conditions for the x axis are described in the caption of Fig. 3.

the required independence of μ_s' from absorber concentration is retained. On the other hand, the analysis of the semi-infinite-measurement data with the infinite-geometry equations yields poor results for both μ_a and μ_s' . μ_a typically deviates by 15% from the accurate values, whereas μ_s' shows a dependence on the absorber concentration. Obviously the use of the infinite-geometry model for analyzing the semi-infinite-geometry data is not expected to yield good results. Nevertheless the comparison presented in Figs. 4 and 5 allows us quantitatively to evaluate the correction that is due to the semi-infinite geometry model. From Fig. 5 one can see that for absorber concentrations smaller than 3 mL/L, which correspond to $\mu_s'/\mu_a > 80$, the use of the semi-infinite-geometry boundary conditions gives rise to corrections in the right direction: the dc, the ac, and the phase slopes are systematically closer to the correct value. For ink concentrations higher than 3 mL/L ($\mu_s'/\mu_a < 80$) the corrections are less precise, especially in the case of the ac slopes.

The Monte Carlo simulation provides an independent test of the semi-infinite-geometry boundary problem. The results presented in Fig. 6 and Table 2 are similar to the ones obtained experimentally. Use of the semi-infinite-geometry boundary conditions yields better accuracy for μ_a than for μ_s' . The corrections provided by the boundary conditions are particularly evident and effective in the evaluation of μ_a . The slopes of the straight lines associated with dc, ac, and phase are closer to the accurate ones when the boundary conditions are applied.

7. CONCLUSIONS

In this paper a systematic study of the applicability of the diffusion approximation to the semi-infinite-geometry boundary problem has been presented. The principal result is that in a macroscopically homogeneous, multiply scattering medium reasonably good estimates of the optical parameters are obtained from the diffusion theory, provided that the appropriate boundary conditions are applied. The fact, also shown in this paper, that the measurements are quite insensitive to the precise geometrical configuration at the surface, namely, the positions of the source and the detector relative to the surface plane of the medium, suggests that slightly different boundary geometries could be equally well represented.

ACKNOWLEDGMENTS

The experimental investigation, as well as the analysis of the data, was performed at the Laboratory for Fluorescence Dynamics (LFD) in the Department of Physics at the University of Illinois at Urbana-Champaign (UIUC). The LFD is supported jointly by the Division of Research Resource of the National Institutes of Health (RR03155) and UIUC, and this research was supported by Grant CA 57032 (to E. Gratton). The authors thank William Mantulin for useful discussions and the critical reading of the manuscript.

*Permanent Address, Istituto di Elettronica Quantistica—Consiglio Nazionale delle Ricerche, Via Panciatichi, 56/30, 50127 Firenze, Italy.

REFERENCES

1. S. Chandrasekhar, *Radiative Transfer* (Oxford U. Press, New York, 1960).
2. V. V. Sobolev, *A Treatise on Radiative Transfer* (Van Nostrand-Reinhold, Princeton, N.J., 1963).
3. K. M. Case and P. F. Zweifel, *Linear Transport Theory* (Addison-Wesley, Reading, Mass., 1967), pp. 196–199.
4. J. J. Duderstadt and L. J. Hamilton, *Nuclear Reactor Analysis* (Wiley, New York, 1976).
5. A. Ishimaru, *Wave Propagation and Scattering in Random Media* (Academic, New York, 1978), Vol. I.
6. K. Furutsu, "Diffusion equation derived from space-time transport equation," *J. Opt. Soc. Am.* **70**, 360–366 (1980).
7. W. F. Cheong, S. A. Prahl, and A. J. Welch, "A review of the optical properties of biological tissues," *IEEE J. Quantum Electron.* **26**, 2166–2185 (1990).
8. J. L. Karagiannes, Z. Zhang, B. Grossweiner, and L. I. Grossweiner, "Applications of the 1-D diffusion approximation to the optics of tissues and tissue phantoms," *Appl. Opt.* **28**, 2311–2317 (1989).
9. P. Parsa, S. L. Jacques, and N. S. Nishioka, "Optical properties of rat liver between 350 and 2200 nm," *Appl. Opt.* **28**, 2325–2330 (1989).
10. T. J. Farrel, M. S. Patterson, and B. Wilson, "A diffusion theory model of spatially resolved, steady-state diffuse reflectance for the noninvasive determination of tissue optical properties *in vivo*," *Med. Phys.* **19**, 879–888 (1992).
11. E. M. Sevick, B. Chance, J. Leigh, S. Nioka, and M. Maris, "Quantitation of time- and frequency-resolved optical spectra for the determination of tissue oxygenation," *Anal. Biochem.* **195**, 330–351 (1991).
12. M. S. Patterson, B. Chance, and B. C. Wilson, "Time resolved reflectance and transmittance for the noninvasive measurement of tissue optical properties," *Appl. Opt.* **28**, 2331–2336 (1989).
13. M. Cope, P. van der Zee, M. Essenpreis, S. R. Arridge, and D. T. Delpy, "Data analysis methods for near infrared spectroscopy of tissues: problems in determining the relative cytochrome *aa*₃ concentration," in *Time-Resolved Spectroscopy and Imaging of Tissues*, B. Chance and A. Katzir, eds., *Proc. Soc. Photo-Opt. Instrum. Eng.* **1431**, 251–263 (1991).
14. D. A. Benaron and D. K. Stevenson, "Optical time-of-flight and absorbance imaging of biologic media," *Science* **259**, 1463–1466 (1993).
15. D. A. Benaron, C. D. Kurth, J. Steven, L. C. Wagerle, B. Chance, and M. Delivoira-Papadopoulos, "Non-invasive estimation of cerebral oxygenation and oxygen consumption using phase-shift spectrophotometry," *Proc. IEEE Eng. Biol. Soc.* **12**, 2004–2006 (1990).
16. W. M. Star, J. P. A. Marijnissen, and M. J. C. van Gemert, "Light dosimetry in optical phantoms and in tissues: I. Multiple flux and transport theory," *Phys. Med. Biol.* **33**, 437–454 (1988).
17. M. S. Patterson, J. D. Moulton, B. C. Wilson, K. W. Berndt, and J. R. Lakowicz, "Frequency-domain reflectance for the determination of the scattering and absorption properties of tissue," *Appl. Opt.* **30**, 4474–4476 (1991).
18. B. J. Tromberg, L. O. Svaasand, T. T. Tsay, and R. C. Haskell, "Properties of photon density waves in multiple-scattering media," *Appl. Opt.* **32**, 607–616 (1993).
19. S. Fantini, M. A. Franceschini, J. B. Fishkin, B. Barbieri, and E. Gratton, "Quantitative determination of the absorption spectra of chromophores in strongly scattering media: a novel LED based technique," *Appl. Opt.* **33**, 5204–5213 (1994).
20. J. B. Fishkin and E. Gratton, "Propagation of photon-density waves in strongly scattering media containing an absorbing semi-infinite plane bounded by a straight edge," *J. Opt. Soc. Am. A* **10**, 127–140 (1993).
21. B. J. Tromberg, L. O. Svaasand, T. T. Tsay, R. C. Haskell, and M. W. Berns, "Optical property measurement in turbid media using frequency-domain photon migration," in *Future Trends in Biomedical Applications of Lasers*, L. O. Svaasand, ed., *Proc. Soc. Photo-Opt. Instrum. Eng.* **1525**, 52–58 (1991).

22. M. Keijzer, W. M. Star, and P. R. M. Storchi, "Optical diffusion in layered media," *Appl. Opt.* **27**, 1820–1824 (1988).
23. R. A. J. Groenhuis, H. A. Ferwerda, and J. J. Ten Bosch, "Scattering and absorption of turbid materials determined from reflection measurements. 1: Theory," *Appl. Opt.* **22**, 2456–2462 (1983).
24. F. P. Bolin, L. E. Preuss, R. C. Taylor, and R. J. Ference, "Refractive index of some mammalian tissues using a fiber optic cladding method," *Appl. Opt.* **28**, 2297–2302 (1989).
25. G. Eason, A. R. Veitch, R. M. Nisbet, and F. W. Turnbull, "The theory of the back scattering of light by blood," *J. Phys. D* **11**, 1463–1479 (1978).
26. B. A. Feddersen, D. W. Piston, and E. Gratton, "Digital parallel acquisition in frequency domain fluorometry," *Rev. Sci. Instrum.* **60**, 2929–2936 (1989).
27. B. C. Wilson, M. S. Patterson, and B. W. Pogue, "Instrumentation for *in vivo* tissue spectroscopy and imaging," in *Medical Lasers and Systems II*, D. M. Harris and C. M. Penney, eds., *Proc. Soc. Photo-Opt. Instrum. Eng.* **1892**, 132–147 (1993).
28. G. M. Hale and M. R. Querry, "Optical constants of water in the 200-nm to 200- μ m wavelength region," *Appl. Opt.* **12**, 555–563 (1973).